

Predicting Phenotypes from Brain Connection Structure

Subharup Guha

Department of Biostatistics, University of Florida

Rex Jung

Department of Neurology, University of New Mexico Health Sciences Center

David Dunson

Department of Statistical Science, Duke University

Summary. This article focuses on the problem of predicting a response variable based on a network-valued predictor. Our motivation is the development of interpretable and accurate predictive models for cognitive traits and neuro-psychiatric disorders based on an individual's brain connection network (connectome). Current methods reduce the complex, high dimensional brain network into low-dimensional pre-specified features prior to applying standard predictive algorithms. These methods are sensitive to feature choice and inevitably discard important information. Instead, we propose a nonparametric Bayes class of models that utilize the entire adjacency matrix defining brain region connections to adaptively detect predictive algorithms, while maintaining interpretability. The Bayesian Connectomics (BaCon) model class utilizes Poisson-Dirichlet processes to find a lower-dimensional, bidirectional (covariate, subject) pattern in the adjacency matrix. The small n , large p problem is transformed into a "small n , small q " problem, facilitating an effective stochastic search of the predictors. A spike-and-slab prior for the cluster predictors strikes a balance between regression model parsimony and flexibility, resulting in improved inferences and test case predictions. We describe basic properties of the BaCon model and develop efficient algorithms for posterior computation. The resulting methods are found to outperform existing approaches and applied to a creative reasoning data set.

Keywords: BaCon; Connectomics; Mixture model; Network data; Neuroscience; Nonparametric Bayes

1. Introduction

Advances in non-invasive brain imaging technologies have made available brain connectivity data at increasingly greater accuracies and spatial resolution. These advances have shifted the focus of neuroscience research away from specialized brain regions having independent effects on cognitive functions (Fuster, 2000) towards brain connectivity networks (or *connectomes*) in which cognitive processes operate as interconnected circuits (Bressler and Menon, 2010). Stirling and Elliott (2008), Craddock et al. (2013) and Wang et al. (2014) provide an overview of relevant technological developments, such as diffusion tensor imaging (DTI), structural magnetic resonance imaging (sMRI) and magnetization-prepared gradient-echo (MP-RAGE).

This paper is motivated by investigations that seek to discover the relationship between brain connectivity structure and a subject-specific response, such as a quantitative creative reasoning score, the presence or absence of a neuropsychiatric disease, or type of ability. For individuals $i = 1, \dots, n$, the data consist of the categorical or quantitative response y_i and the undirected connectivity network among V brain regions, represented by a binary $V \times V$ symmetric adjacency matrix, $\mathbf{A}_i = ((a_{ij_1j_2}))$. For $j_1, j_2 = 1, \dots, V$, binary element $a_{ij_1j_2}$ equals 1 if and only if at least one white matter fiber connects brain regions j_1 and j_2 in subject i . In some investigations, a vector of subject-specific covariates \mathbf{r}_i is also available.

We focus on the MRN-114 dataset available at <http://openconnecto.me/data/public/MR/>. The responses y_1, \dots, y_n of $n = 114$ individuals are creative reasoning scores measured using the composite creativity index (CCI) (Jung et al., 2010). The brain region adjacency information for these individuals, available from structural MP-RAGE and DTI brain scans (Roncal et al., 2013), consists of $V = 70$ network nodes corresponding to brain regions by the Desikan atlas (Desikan et al., 2006) and equally divided between the left and right hemisphere.

The goal is to identify clusters of brain connections operating in tandem, identify a sparse set of connections capable of explaining individual variations in CCI, and make reliable CCI predictions for out-of-the-bag individuals for whom only brain architecture

information is available. These are challenging tasks, especially because the $70(70 - 1)/2 = 2,415$ brain region pairs overwhelm the number of individuals, making it a “small n , large p ” statistical problem.

Existing methods for categorical responses in brain connectivity problems. Several methods have been developed for classification based on the brain networks of individuals; see Bullmore and Sporns (2009) and Stam (2014) for an overview. A majority of these methods reduce individual connectivity information to prespecified summaries that characterize the network, e.g., number of connections, average path length, and clustering coefficient (Rubinov and Sporns, 2010). These features are then used in standard classification algorithms such as support vector machines. Unfortunately, the results are highly sensitive to the chosen summary measures and often ignore additional brain connectivity information contributing to individual or group differences. Refer to Arden et al. (2010) for examples of inconsistencies in analyses relating brain connectivity networks to creative reasoning.

An alternative strategy avoids discarding useful connectome information by testing for differences between groups in each brain region pair, while adjusting for multiple testing via false discovery rate (FDR) control (Genovese et al., 2002). However, because there are $V(V - 1)/2$ distinct pairs of brain regions, the number of tests is large when $V = 70$. Since they ignore network information, these univariate approaches tend to have low power (Fornito et al., 2013) and substantially underestimate brain connectivity variation across groups. Some methods attempt to compensate for this by replacing the usual Benjamini and Hochberg (1995) approach with thresholding procedures utilizing network information (e.g., Zalesky et al., 2010). Such approaches require careful interpretation and their parameters must be meticulously chosen to give reliable results.

Durante et al. (2018) incorporate network information into their Bayesian model. This is accomplished by expressing the joint pmf of the data (y_i, \mathbf{A}_i) , $i = 1, \dots, n$, as the product of the marginal pmf of group y_i and the conditional pmf for matrix \mathbf{A}_i given the group. This approach facilitates testing of the association between connectivity and the categorical response, while borrowing information across subjects in learning the

network structure.

Graph convolutional networks are promising approaches that leverage the topology of brain networks. Recently, Liu et al. (2019) developed a nonlinear latent factor model for summarizing the brain graph in unsupervised and supervised settings. The approach, called Graph AuTo-Encoding (GATE), relies on deep neural networks and is extended to regression with GATE (reGATE) to relate human phenotypes with brain structural connectivity.

1.1. Inference goals

This paper proposes a nonparametric Bayes method capable of analyzing categorical responses as well as quantitative responses such as continuous measurements and counts. For individual $i = 1, \dots, n$, the binary values $\{a_{ij_1j_2} : j_1 > j_2 \text{ and } j_1, j_2 = 1, \dots, V\}$ representing the pairwise connectivity of the brain regions are vectorized as covariates x_{i1}, \dots, x_{ip} , where $p = V(V - 1)/2$. This equivalent representation of the n adjacency matrices gives an n by p matrix \mathbf{X} consisting of n -variate column vectors denoted by $\mathbf{x}_j = (x_{1j}, \dots, x_{nj})'$, $j = 1, \dots, p$.

From this perspective, the goals of the analysis can be restated as follows: *(i) Cluster detection:* We wish to identify latent clusters of covariates having similar patterns for the subjects. As suggested by Bressler and Menon (2010), these clusters may represent unknown cognitive processes consisting of brain region pairs operating as interconnected circuits; *(ii) Identification of sparse regression models:* From the p brain region pairs, we wish to detect a reliable and parsimonious regression model for the responses; *(iii) Response prediction:* Using the inferred regression model, we wish to predict the responses of additional subjects for whom only connectome information is available. Because we are interested in the relationship between the covariates and responses, as a pre-processing step, we discard any constant covariates (i.e., vectors of all n zeros or all n ones). In the MRN-114 dataset, this gives $p = 1,374$ covariate vectors.

Some existing Bayesian approaches. Outside the realm of connectome applications, there are general Bayesian strategies for achieving one or more of the analytical goals.

However, since most of these techniques were not specifically designed for small n , large p problems, methods are being continually developed to meet the statistical and computational challenges posed by newer applications and larger datasets.

Bayesian clustering techniques typically rely on the ubiquitous Dirichlet process (e.g. see Müller and Mitra, 2013, chap. 4). Lijoi, Mena, and Prünster (2007a) recommended Gibbs-type priors (Gnedin and Pitman, 2005; Lijoi, Mena, and Prünster, 2007b), such as Poisson-Dirichlet processes, for more flexibly fitting cluster structures and demonstrated their utility in some biomedical applications. More recently, Guha and Baladandayuthapani (2016) introduced a clustering and variable selection technique for high dimensional datasets with continuous covariates such as gene expression. This technique is not directly applicable to structural connectivity datasets with binary covariates, which require a very different approach. Motivated by these challenges, we propose a novel Bayesian clustering technique for binary covariates in small n , large p problems that discovers the complex relationships between brain connectivity and subject-specific phenotypes.

O’Hara and Sillanpää (2009) have reviewed Bayesian variable selection techniques in linear and non-linear regression models. For Gaussian responses, common linear methods include stochastic search variable selection (George and McCulloch, 1993), selection-based priors (Kuo and Mallick, 1997), and shrinkage-based methods (Park and Casella, 2008; Xu et al., 2015; Griffin et al., 2010). Empirical Bayes methods include Yengo et al. (2014), who model the regression coefficients using a Gaussian mixture model. These regression methods make strong parametric assumptions and do not account for collinearity commonly observed in high dimensional datasets. Some linear regression approaches allow nonparametric distributions for the error residuals (Hanson and Johnson, 2002; Kundu and Dunson, 2014) and regression coefficients (Bush and MacEachern, 1996; MacLehose and Dunson, 2010).

Challenges in high dimensional settings. Variable selection is particularly challenging in structural connectivity datasets because of the high degree of similarity among the p covariates. Figure 1 displays the histogram of mean taxicab distances for the $p(p-1)/2 = 943,251$ covariate pairs of the MRN-114 dataset. For binary-valued covariate vectors,

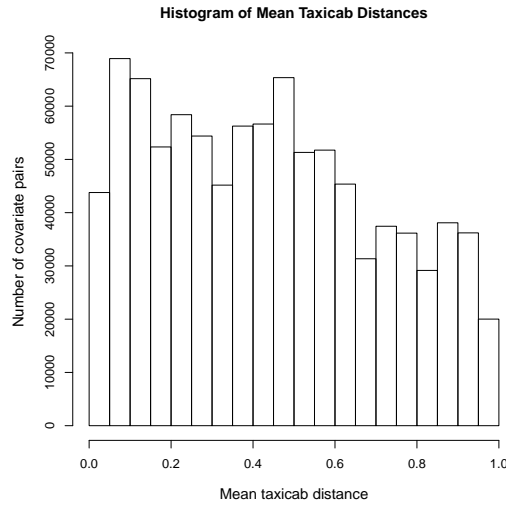


Fig. 1. For the MRN-114 dataset, mean taxicab distances between the $p = 1,374$ non-constant covariate vectors of length $n = 114$ each.

a natural measure of similarity is the mean taxicab distance, which is a proportion lying between 0 and 1. A mean taxicab distance of 0 (1) corresponds to a perfect match (mismatch) between the n elements of two binary vectors. The 25th percentile of the mean taxicab distances in Figure 1 is 0.2018, and the distribution is skewed left, indicating substantial similarity between the covariate vectors.

This is a pervasive problem not only in connectome datasets, but more generally in small n , large p problems. It occurs because the n -dimensional space of the covariate columns is saturated with the much larger number of covariates. Moreover, collinearity makes it difficult to find a good set of predictors in regression settings. Collinearity also causes unstable inferences and erroneous test case predictions (Weisberg, 1985), rendering many of the aforementioned techniques ineffectual in brain connectivity applications.

This paper proposes BaCon (an acronym for Bayesian Connectomics), a fundamentally different approach for connectome applications. The technique specifies a joint model for the covariates and responses and introduces new Bayesian nonparametric methodology for the unsupervised clustering of binary covariates. This innovation has the twin benefits of achieving dimension reduction and overcoming collinearity issues.

Bidirectional clustering with regression variable selection and prediction. BaCon uses Poisson-Dirichlet processes (PDPs) to group the p columns of the covariate matrix into q latent clusters, where q is much smaller than p . Each cluster consists of covariate columns that are similar but not necessarily identical. The covariates belonging to a cluster are modeled as contaminated cluster-specific latent vectors; the notion of “contamination” is precisely defined in Section 2. The taxicab distances between covariates belonging to a cluster are typically small, with occasional mismatches for a small number of individuals. The data are permitted to choose between PDPs and their special case, a Dirichlet process, for an appropriate covariate-to-cluster allocation scheme. To flexibly capture the shared latent binary pattern of the covariates within a cluster, each cluster allows the individuals to group differently via nested Bernoulli mixtures. This feature of the model is motivated by biomedical studies (e.g., Jiang et al., 2004) which have broadly demonstrated that subjects tend to group differently under different biological processes.

The proposed analytical framework detects a lower-dimensional, bidirectional (covariate, subject) clustering pattern in the binary covariates. The small n , large p problem is thereby transformed into a “small n , small q ” problem, facilitating an effective stochastic search of the predictors. A spike-and-slab prior for the cluster predictors strikes a balance between regression model parsimony and flexibility, resulting in improved inferences and test case predictions.

Figure 2 illustrates the main concepts using a toy example with $n = 10$ subjects and $p = 25$ covariates, with the zero covariates depicted as white and the ones as grey. The responses are continuous measurements, like the CCIs in the MRN-114 dataset. The plot in the upper left panel depicts the covariates. The posterior analysis averages over realizations of two basic stochastic steps:

- (a) **Clustering** The column vectors are assigned, based on similarity, to $q = 9$ PDP-Bernoulli mixture clusters. The shuffled covariate columns are plotted in the upper right panel. Notice that covariates mapped to a cluster are similar but not necessarily identical.
- (b) **Variable selection and regression** One covariate called the *cluster representative* is stochastically selected from each cluster. The regression predictors

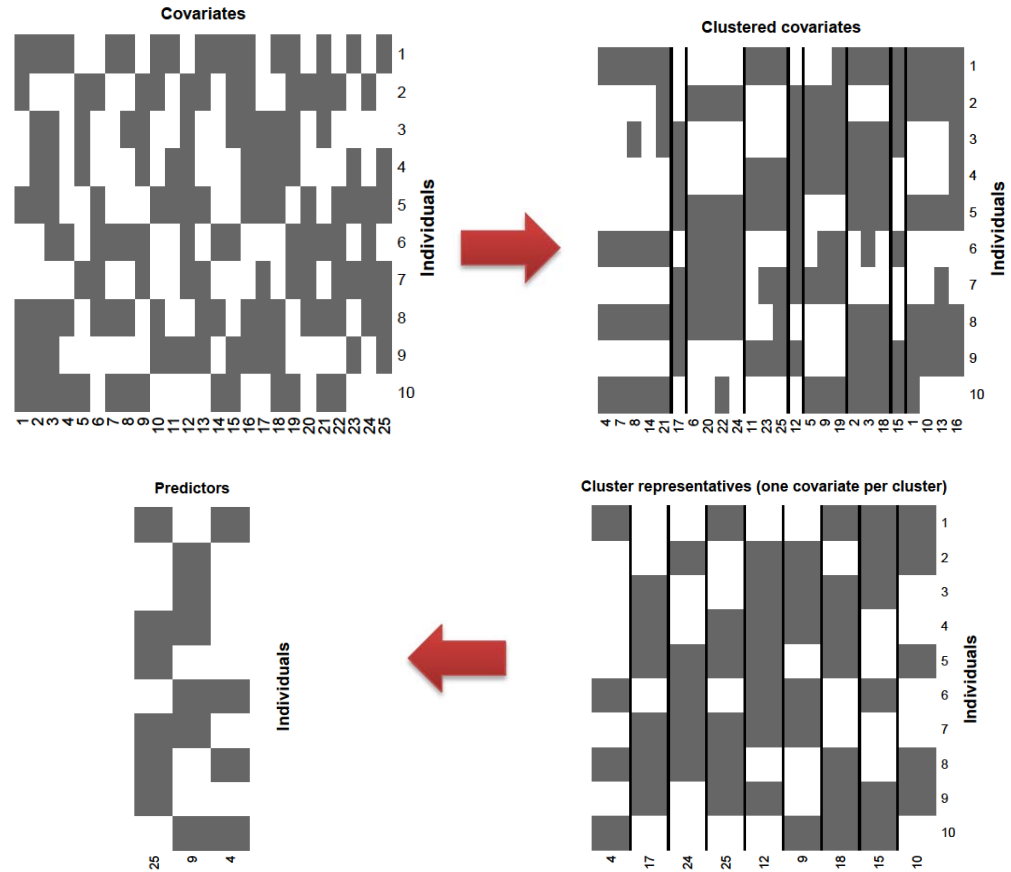


Fig. 2. Stylized example illustrating the key ideas of BaCon for $n = 10$ subjects and $p = 25$ covariates. The covariates belong to $q = 9$ number of latent PDP clusters. The covariate indices are the column labels and the subjects are the row labels. Zero covariate values are shown in white and ones are shown in grey. The inferred regression relationship in the above situation is $Y = \beta_0 + \beta_1 X_4 + \beta_6 X_9 + \beta_4 X_{25} + \epsilon$, where the regression coefficient subscripts are the cluster labels of the predictors. See the text for further explanation.

are chosen from this set. The middle panel displays the cluster representatives, $\mathbf{x}_4, \mathbf{x}_{17}, \mathbf{x}_{24}, \mathbf{x}_{25}, \mathbf{x}_{12}, \mathbf{x}_9, \mathbf{x}_{18}, \mathbf{x}_{15}$, and \mathbf{x}_{10} . Only a few representatives are response predictors. The predictors, $\mathbf{x}_{25}, \mathbf{x}_9$, and \mathbf{x}_4 , are shown in the lower panel. For a zero-mean Gaussian error ϵ , the regression equation is $Y = \beta_0 + \beta_1 X_4 + \beta_6 X_9 + \beta_4 X_{25} + \epsilon$. The β parameter subscripts are the cluster labels, e.g., coefficient β_1 is the effect of the first PDP cluster to which representative \mathbf{x}_4 belongs.

In applications where an interpretable regression model is not of primary interest, alternative variable selection strategies discussed in Section 2.2 can be applied.

The rest of the paper is organized as follows. Section 2 formally describes the BaCon model. Section 3 outlines the inference procedure. The substantial benefits and accuracy of BaCon are demonstrated by simulation studies in Section 4. The motivating connectome dataset, MRN-114, is analyzed in Section 5.

2. The BaCon Model

The statistical model is motivated by the three-pronged goals of the analysis described in Section 1.1. Dimension reduction in the $p = V(V - 1)/2$ number of brain region pairs is achieved by Poisson-Dirichlet processes (PDPs), which allow a greater variety of clustering patterns than Dirichlet processes. The PDP allocations group the p covariates into a smaller number of latent clusters. All covariate columns assigned to a cluster share a common n -variate pattern called the *latent vector*. Occasionally, a random misclassification may occur at a given position of a covariate vector, causing the binary digit for that position (i.e., individual) to toggle relative to the latent vector element. From this perspective, the covariates may be regarded as contaminated versions of their cluster’s latent vector.

2.1. Covariate clusters

We assume that each column vector \mathbf{x}_j belongs to exactly one of $q \ll p$ latent clusters, where the cluster memberships and q are unknown. For the covariate $j = 1, \dots, p$ and cluster $k = 1, \dots, q$, the covariate-to-cluster assignment is determined by an *allocation*

variable c_j , which equals k if the j th covariate belongs to the k th latent cluster. The q clusters are associated with latent vectors $\mathbf{v}_1, \dots, \mathbf{v}_q$ of length n , where each latent vector element $v_{ik} \in \{0, 1\}$.

We model the covariate allocations as partitions induced by the *two-parameter Poisson-Dirichlet process*, $\mathbb{PDP}(M, d)$, with discount parameter $0 \leq d < 1$ and mass parameter $M > 0$. PDPs were introduced by Perman et al. (1992) and further studied by Pitman (1995) and Pitman and Yor (1997). The PDP covariate-cluster assignment can be described by an extension of the well-known Chinese restaurant process metaphor: Imagine customers, representing the covariates, arriving at a restaurant. The first customer sits at a table labeled 1 (without loss of generality) so that $c_1 = 1$. The second customer may sit at table 1 with probability $(1 - d)/(M + 1)$ or sit at a new table having label 2 with probability $(M + d)/(M + 1)$. The table eventually selected by customer 2 is recorded as c_2 . The process proceeds in this manner. For customers $j = 3, \dots, p$, suppose there exist $q^{(j-1)}$ occupied tables among the current customer-table assignments c_1, \dots, c_{j-1} , with $n_k^{(j-1)}$ customers currently seated at the k th occupied table. The probability that the j th customer sits at the k th table is

$$P(c_j = k \mid c_1, \dots, c_{j-1}) \propto \begin{cases} n_k^{(j-1)} - d & \text{if } k = 1, \dots, q^{(j-1)} \\ M + q^{(j-1)} \cdot d & \text{if } k = q^{(j-1)} + 1 \end{cases}$$

where the event $c_j = q^{(j-1)} + 1$ in the second line corresponds to the j th customer selecting a new table, which is then assigned the label $q^{(j-1)} + 1$. Eventually, the sequence of customer-table selections is represented by allocation variables c_1, \dots, c_p . The tables occupied by the p customers represent the $q = q^{(p)}$ latent clusters, and the customers seated at the k th occupied table represent the covariates allocated to the k th cluster.

Despite the sequential description of the extended Chinese restaurant metaphor, it can be shown that the p allocation variables are a priori exchangeable for PDPs, and more generally, also for product partition models (Barry and Hartigan, 1993; Quintana and Iglesias, 2003) and species sampling models (Ishwaran and James, 2003). The number of distinct clusters, q , is stochastically increasing in the PDP parameters M and d . For

fixed d , all p covariates are assigned to singleton clusters (i.e., $q = p$) in the limit as $M \rightarrow \infty$. When $d = 0$, we obtain the Dirichlet process with mass parameter M . Refer to Lijoi and Prünster (2010) for a detailed discussion of Bayesian nonparametric models, including Dirichlet processes and PDPs.

PDPs allow effective dimension reduction in high dimensional settings; the random number of clusters, $q = q^{(p)}$, is asymptotically equivalent to

$$\begin{cases} M \log p & \text{if } d = 0 \quad (\text{Dirichlet process}) \\ S_{d,M} p^d & \text{if } 0 < d < 1 \end{cases} \quad (1)$$

where $S_{d,M}$ is a positive random variable. The number of clusters is asymptotically smaller order than p , resulting in dimension reduction when p is large. Equation (1) implies that the number of clusters for a Dirichlet process is smaller order than for a PDP. Dirichlet processes have been previously utilized for dimension reduction; for example, see Medvedovic et al. (2004), Kim et al. (2006), Dunson et al. (2008), and Dunson and Park (2008). The discount parameter d is given mixture prior $\frac{1}{2}\delta_0 + \frac{1}{2}U(0, 1)$, where δ_0 denotes a point mass at 0. Although we suspect that connectome datasets may be more appropriately modeled with PDPs, this specification is appealing in allowing the model to adaptively simplify to a Dirichlet process when appropriate.

Latent vector elements. The PDP prior specification is completed by a *base distribution* in $\{0, 1\}^n$ for each binary latent vector. We assume that the nq elements of latent vectors $\mathbf{v}_1, \dots, \mathbf{v}_q$ are distributed as

$$v_{ik} \stackrel{iid}{\sim} \text{Bernoulli}(p_*), \quad i = 1, \dots, n, \quad k = 1, \dots, q, \quad (2)$$

allowing the clusters and individuals to communicate through a shared parameter which is given a conjugate prior:

$$p_* \sim \text{Beta}(\lambda/2, \lambda/2), \quad \lambda > 0. \quad (3)$$

The PDP base distribution is the n -fold product measure of this Bernoulli distribution. We denote by $q_* = 1 - p_*$ the prior probability of a latent vector element being 0.

The PDP allocations and mixture assumptions (2) and (3) for the latent vectors induce a nested clustering of the np covariates. Unlike the clustering approaches for continuous covariates proposed by Fraley and Raftery (2002), Quintana (2006) and Freudenberg et al. (2010), we do not assume that it is possible to *globally* reshuffle the rows and columns of the data matrix to reveal a clustering pattern. Instead, somewhat similar to the nonparametric Bayesian local clustering (NoB-LoC) approach of Lee et al. (2013), we cluster the covariates locally using two sets of mixture models (Hartigan, 1990; Barry and Hartigan, 1993; Crowley, 1997). However, there are significant differences in that our approach is primarily suited for binary rather than continuous covariates. Furthermore, NoB-LoC relies solely on two sets of Dirichlet processes, whereas BaCon relies on Bernoulli mixtures nested within a PDP.

Relating the covariates to the latent clusters Let the j th covariate be allocated to the k th cluster, so that $c_j = k$. As mentioned, the individual elements of column vector \mathbf{x}_j arise as possibly corrupted versions of the k th latent vector's elements with a high probability of non-contamination (i.e., $x_{ij} = v_{ik}$). This results in similar patterns of covariates belonging to a cluster. Conditional on latent vector element $v_{ik} = s \in \{0, 1\}$, covariate x_{ij} has the distribution

$$P(x_{ij} = t \mid c_j = k, v_{ik} = s, \mathbf{Q}) = q_{st}, \quad \text{where } t = 0, 1, \quad (4)$$

for a 2×2 matrix of *contamination probabilities* $\mathbf{Q} = ((q_{st}))$. High levels of agreement between the covariates and latent vectors are ensured by the diagonal elements of the matrix \mathbf{Q} being close to 1. This, in turn, implies tight clusters with high levels of concordance between member covariates. From a broader statistical perspective, the idea of modeling the units in a cluster as contaminated versions of latent cluster-specific characteristics is not new; for example, see Dunson (2009) for a nonparametric Bayesian technique that allows dependent local clustering and borrowing of information using Dirichlet process priors.

Row vectors \mathbf{q}_0 and \mathbf{q}_1 of the matrix \mathbf{Q} sum to 1. They are assigned independent priors on the unit simplex in \mathcal{R}^2 as follows. Let $\mathcal{I}(\cdot)$ be the indicator function and let

$\mathbf{1}_s$ be the $(s + 1)$ th unit vector in \mathcal{R}^2 , i.e., with the $(s + 1)$ th element equal to 1 and the other elements equal to zero. For $s = 0, 1$, row vector \mathbf{q}_s has the expression

$$\begin{aligned} \mathbf{q}_s &= (q_{s0}, q_{s1}) = r_s \mathbf{1}_s + (1 - r_s) \mathbf{q}_s^*, \quad \text{where row vector} \\ \mathbf{q}_s^* &= (q_{s0}^*, q_{s1}^*) \sim \mathcal{D}_2(\alpha/2, \alpha/2), \quad \text{and} \\ r_s &\sim \text{beta}(r_\alpha, r_\beta) \cdot \mathcal{I}(r_s > r^*), \end{aligned} \tag{5}$$

for prespecified constants r^* , r_α and r_β , and with \mathcal{D}_2 representing a Dirichlet distribution on the unit simplex in \mathcal{R}^2 . Specification (5), along with the assumption that $r^* > 0.5$, guarantees that matrix \mathbf{Q} is diagonally dominant. We refer to r_s as the s th *concordance parameter*. Since the concordance parameters determine the cluster separation, we set $r^* = 0.85$ to facilitate the detection of tight clusters.

2.2. Regression and prediction

Continuous, categorical or count outcomes. If the subject-specific responses are non-Gaussian, denote them by w_1, \dots, w_n . The Laplace approximation (Harville, 1977) transforms the responses w_i to independent regression outcomes y_i having possibly approximate distributions, $N(\eta_i, \sigma_i^2)$. For an appropriate link function $g(\cdot)$, the normal mean $\eta_i = g(E[w_i])$. Laplace-type approximations are routinely used in exponential family models (Zeger and Karim, 1991; Albert and Chib, 1993). Gaussian, Poisson, negative binomial, and binomial responses all belong to this setting. The approximation is exact for Gaussian responses (e.g., CCI responses in the MRN-114 dataset), which correspond to the identity link function and have a common $\sigma = \sigma_i$ for all n individuals.

Cluster-based covariate selection. Suppose n_k covariates are allocated to the k th cluster. To mitigate collinearity effects, we assume that each cluster elects from its member covariates a *representative*, denoted by \mathbf{u}_k . A subset of the q cluster representatives, rather than of the p covariates, feature in an additive regression model. The cluster representatives may be chosen in several different ways depending on the application. Some possible options are:

- (a) Select with apriori equal probability one of the n_k covariates belonging to the k th cluster. If covariate s_k is selected as the representative, then $c_{s_k} = k$ and $\mathbf{u}_k = \mathbf{x}_{s_k}$.
- (b) We may find that some covariates belonging to a cluster closely resemble the shared cluster pattern while others are barely in the cluster. It may then be preferable to pick as the cluster representative the *within-cluster median covariate*, the covariate having the minimal sum of distances to the other covariates.
- (c) Select cluster-specific latent vector \mathbf{v}_k as the cluster representative.

Option (a) is more relevant when practitioners are interested in interpretable models identifying the effects of relevant regressors, i.e., brain region pairs. Option (b) may be preferred when the emphasis is more on identifying clusters of variables (e.g., cognitive processes) jointly influencing the responses.

Extensions of spike-and-slab priors (George and McCulloch, 1993; Kuo and Mallick, 1997; Brown et al., 1998) are applied in selecting the regression predictors from the q cluster representatives:

$$y_i \stackrel{indep}{\sim} N(\eta_i, \sigma_i^2), \quad \text{where}$$

$$\eta_i = \beta_0 + \sum_{k=1}^q \gamma_k \beta_k u_{ik} \quad (6)$$

When the Laplace approximation is applied to the response w_i to model regression outcome y_i , variance σ_i^2 may depend on i , as in Poisson and binomial responses. If an additional vector of known predictors \mathbf{r}_i is available, it could be included in regression equation (6) along with its regression coefficients.

The linear predictor η_i in expression (6) relies on a vector of cluster-specific indicators, $\boldsymbol{\gamma} = (\gamma_1, \dots, \gamma_q)$. If $\gamma_k = 0$, none of the covariates belonging to cluster k are associated with the response. If $\gamma_k = 1$, cluster representative \mathbf{u}_k appears as a regressor in equation (6). The number of clusters associated with the response is then $q_1 = \sum_{j=1}^q \gamma_j$. The remaining $q_0 = q - q_1$ clusters are not associated with the response. For example, consider again Figure 2, where one covariate from each cluster is the representative, as described above in Option (i). Of the $q = 9$ cluster representatives, $q_1 = 3$ are predictors

and the remaining $q_0 = 6$ are non-predictors.

The following truncated prior for indicator vector γ ensures model sparsity:

$$[\gamma] \propto (1 - \omega_1)^{q - q_1} \omega_1^{q_1} \cdot \mathcal{I}(q_1 < n - 1), \quad \text{where}$$

$$\omega_1 \sim \text{beta}(1, 1). \quad (7)$$

Conditional on the variances σ_i^2 in equation (6), we assume a weighted g prior for the regression coefficients of the predictors:

$$\beta_\gamma | \Sigma \sim N_{q+1} \left(\mathbf{0}, \sigma_\beta^2 (\mathbf{U}_\gamma' \Sigma^{-1} \mathbf{U}_\gamma)^{-1} \right), \quad \text{where}$$

$$\Sigma = \text{diag}(\sigma_1^2, \dots, \sigma_n^2). \quad (8)$$

2.3. Justification of the clustering mechanism

We discuss the suitability of using PDPs as a covariate clustering device and an interesting consequence.

Empirical evidence against Dirichlet processes. In an exploratory data analysis (EDA) of brain region connectivity in the motivating MRN-114 dataset, the $p = 1,374$ non-constant covariate vectors were grouped in an ad hoc manner to detect the clusters. Specifically, we iteratively applied the k-means procedure to cluster the covariates until the within-cluster median taxicab distances of the covariates were less than 0.4 for all the clusters. The observed allocation pattern, shown in Figure 3, is highly uncharacteristic of Dirichlet processes; as is well known, Dirichlet processes are associated with relatively small numbers of clusters with exponentially decaying cluster sizes. The large number of clusters ($\hat{q} = 344$) and the predominance of small clusters in Figure 3 suggest a non-Dirichlet covariate-cluster assignment. PDPs are an attractive option because of their tractability, larger number of clusters, and the slower, power law decay of their cluster sizes. For the MRN-114 dataset, the best-fitting power law function, $102.5k^{-0.74}$, $k > 1$, is shown in Figure 3. However, we prefer a flexible general specification that allows the data to choose between a PDP or Dirichlet process. Hence, as described in

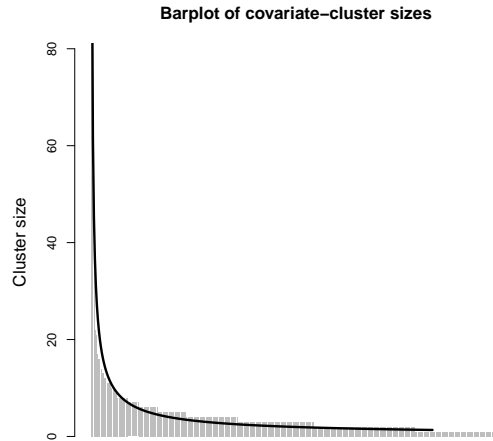


Fig. 3. Cluster sizes in the MRN-111 dataset detected by EDA. The best-fitting power law curve is overlaid in black.

Section 2.1, we choose a mixture prior for the PDP parameter d with a point mass at zero corresponding to the Dirichlet process.

Theoretical consequences and justifications for a PDP model. BaCon’s nested mixture model cluster structure has some interesting consequences. The n -variate base distribution of the PDP is discrete, and there is a positive probability that two clusters have identical latent vectors. However, an upper bound of the probability that two or more of the q PDP clusters have identical latent vectors is $\binom{q}{2} (p_*^2 + q_*^2)^n$, with p_* and q_* defined in expression (3). Applying asymptotic relationship (1), we find that the upper bound approaches 0 as the dataset grows, provided the number of covariates, p , grows at a slower-than-exponential rate with n . Even for moderate-sized datasets with $n = 50$ and $p = 250$, all the latent vectors were distinct in our data analyses and simulation studies. Consequently, it is reasonable to assume that all BaCon clusters have unique features in structural connectivity datasets.

3. Posterior inference

Starting with ad hoc estimates, the BaCon model parameters are iteratively updated by MCMC methods. The post–burn-in MCMC sample is used for posterior inference. As a benefit of having a coherent stochastic model, we are able to appropriately incorporate uncertainty into the inferences. Due to the computationally intensive MCMC procedure, the analysis is performed in separate steps, consisting of dimension reduction in the covariates followed by variable selection.

Step 1 Focusing only on the binary connectivity information for the brain regions:

Step 1(i) The allocation variables, latent vector elements, and all model parameters directly related to the covariates are updated until the MCMC chain converges. Section 3.1.1 describes Gibbs sampling updates for the p allocation variables. Section 3.1.2 specifies a Gibbs sampler for the latent vector elements. Sections 3.1.3 describes a Gibbs sampler for the contamination probability matrix, \mathbf{Q} . The remaining hyperparameters, such as the PDP discount parameter d , are generated using standard MCMC techniques.

Monte Carlo estimates are computed for the posterior probability of clustering for each pair of covariates. Following Dahl (2006), these probabilities are used to compute a point estimate, called the *least-squares allocation*, for the PDP assignments.

Step 1(ii) Conditional on the least-squares allocation consisting of \hat{q} PDP clusters, a second MCMC sample of the $n\hat{q}$ latent vector elements is generated. An estimate of these binary latent vector elements, called the *least-squares configuration*, is evaluated by again applying the technique of Dahl (2006).

Step 2 Finally, using the responses, and conditional on the least-squares allocation and least-squares configuration, the regression predictors and any latent regression outcomes are generated to obtain a third MCMC sample. Response predictions are also made for test set individuals (if any).

3.1. MCMC procedure

3.1.1. Covariate-to-cluster allocation

For the j th covariate column, we perform Gibbs sampling updates of PDP allocation variable c_j , $j = 1, \dots, p$. The simulation strategy consists of the following steps:

- (a) Discard parameters exclusively related to the j th covariate. Let q^- be the number of clusters among the remaining $(p - 1)$ allocation variables, with the k th cluster containing n_k^- number of covariates. The j th covariate may join one of the existing q^- clusters or open a new cluster having the label $(q^- + 1)$. We evaluate the probabilities of these events and update parameter c_j as described in Steps (b) – (d).
- (b) For each of the existing clusters, i.e., for $k = 1, \dots, q^-$, compute:
- (i) **Transition counts for the cluster-covariate combination** Compute matrix $\mathbf{N}^{(jk)} = ((n_{st}^{(jk)}))$, the 2×2 table of transition counts, defined as

$$n_{st}^{(jk)} = \sum_{i=1}^n \mathcal{I}(v_{ik} = s, x_{ij} = t), \quad \text{for } s, t = 0, 1. \quad (9)$$

- (ii) **Posterior probability that allocation variable $c_j = k$** The posterior probability of the j th covariate belonging to the k th cluster is proportional to

$$\xi_{jk} = (n_k^- - d) \cdot \prod_{s=0,1} \prod_{t=0,1} q_{st}^{n_{st}^{(jk)}} \quad \text{for } k = 1, \dots, q^-. \quad (10)$$

- (c) **Posterior probability that allocation variable $c_j = q^- + 1$** The posterior probability of the j th covariate opening a new cluster is proportional to

$$\xi_{j(q^-+1)} = (M + q^- d) \cdot \prod_{t=0,1} (q_* q_{0t} + p_* q_{1t})^{n_t^{(j(q^-+1))}} \quad (11)$$

where $n_t^{(j(q^-+1))} = \sum_{i=1}^n \mathcal{I}(x_{ij} = t)$, and q_* and p_* are defined in relation (3).

- (d) **Generation of allocation variable c_j** Using the values computed in expressions (10) and (11), evaluate the constant ξ_j that normalizes to probabilities the

values $\xi_{j1}, \dots, \xi_{j(q^-+1)}$. That is, $\xi_j = 1 / \sum_{k=1}^{q^-+1} \xi_{jk}$. Set the allocation variable c_j equal to k with probability equal to $\xi_j \cdot \xi_{jk}$, or $k = 1, \dots, (q^- + 1)$. If $k = (q^- + 1)$, also generate the latent vector \mathbf{v}_{q^-+1} for the new cluster: conditional on p_* and matrix \mathbf{Q} , the n elements of vector \mathbf{v}_{q^-+1} have a posteriori independent Bernoulli distributions.

3.1.2. Latent vector elements

Among allocation variables c_1, \dots, c_p , suppose there are q clusters with cluster k consisting of $n_k = \sum_{j=1}^p \mathcal{I}(c_j = k)$ covariates. The sufficient statistics for updating the latent vector elements is the n by q matrix of counts, $\mathbf{W} = ((w_{ik}))$, where $w_{ik} = \sum_{j:c_j=k} \mathcal{I}(x_{ij})$. Conditional on parameter p_* and on the matrices \mathbf{Q} and \mathbf{W} , the nq latent vector elements have independent Bernoulli full conditional distributions.

3.1.3. Gibbs sampler for contamination probability matrix \mathbf{Q}

Using the row vectors $\mathbf{q}_s^* = (q_{s0}^*, q_{s1}^*)$ and concordance parameters of relation (5), let the matrix $\mathbf{Q}^* = ((q_{st}^*))$ and concordance parameter vector, $\mathbf{r} = (r_0, r_1)'$. From relation (5), we find that updating the matrix \mathbf{Q} is equivalent to a posteriori generating vector \mathbf{r} followed by updating matrix \mathbf{Q}^* conditional on \mathbf{r} . The details are described below.

Comparing each cluster's latent vector to its allocated covariates, evaluate matrix $\mathbf{N} = ((n_{st}))$, the 2×2 table of transition counts, which is the sufficient statistic for updating matrix \mathbf{Q} . That is, the transition count

$$n_{st} = \sum_{i=1}^n \sum_{j=1}^p \mathcal{I}(v_{ic_j} = s, x_{ij} = t), \quad \text{for } s, t = 0, 1.$$

Updating concordance parameter vector \mathbf{r} For $s = 0, 1$, define the pmf

$$h_s(v) = \begin{cases} g_s(v) / \sum_{u=0}^{n_{ss}} g_s(u) & \text{if } v = 0, \dots, n_{ss}, \\ 0 & \text{otherwise,} \end{cases} \quad (12)$$

which relies on non-negative functions $g_0(\cdot)$ and $g_1(\cdot)$ having the definition:

$$g_s(v) = \begin{cases} \binom{n_{ss}}{v} \frac{B(\mathbf{n}_s + \frac{\alpha}{2}\mathbf{1} - v\mathbf{1}_s)}{B(v+r_\alpha, N_s - v + r_\beta)} \tilde{F}(r^* | v + r_\alpha, N_s - v + r_\beta) & \text{if } v = 0, \dots, n_{ss}, \\ 0 & \text{otherwise,} \end{cases}$$

where \mathbf{n}_s denotes the s th row of matrix \mathbf{N} , $N_s = \sum_{t=0,1} n_{st}$ is the matrix's s th row sum, and $\mathbf{1}$ is the bivariate vector of ones. As defined in equation (3), $\mathbf{1}_s$ is the $(s+1)$ th unit vector in \mathcal{R}^2 . The survival function (i.e., $1 - \text{cdf}$) for the beta distribution with parameters $(v + r_\alpha)$ and $(N_s - v + r_\beta)$ is denoted by $\tilde{F}(\cdot | v + r_\alpha, N_s - v + r_\beta)$. For a bivariate vector $\mathbf{a} = (a_1, a_2)$, beta function $B(\mathbf{a}) = B(a_1, a_2) = \prod_{s=0,1} \Gamma(a_{s+1}) / \Gamma(\mathbf{a}'\mathbf{1})$.

Then, as shown in the Appendix, the concordance parameters are a posteriori independently distributed as truncated beta distributions:

$$r_s | \mathbf{X}, V_s, \dots \stackrel{indep}{\sim} \text{beta}(V_s + r_\alpha, N_s - V_s + r_\beta) \cdot \mathcal{I}(r_s > r^*), \quad \text{where} \\ V_s \stackrel{indep}{\sim} h_s(\cdot), \quad s = 0, 1. \quad (13)$$

Updating matrix \mathbf{Q}^ conditional on concordance parameter vector \mathbf{r}* For $s = 0, 1$, define the pmf

$$l_s(v) = \begin{cases} l_s^*(v) / \sum_{u=0}^{n_{ss}} l_s^*(u) & \text{if } v = 0, \dots, n_{ss}, \\ 0 & \text{otherwise,} \end{cases} \quad (14)$$

where the non-normalized function

$$l_s^*(v) = \begin{cases} \binom{n_{ss}}{v} B(\mathbf{n}_s + \frac{\alpha}{2}\mathbf{1} - v\mathbf{1}_s) \rho_s^v & \text{if } v = 0, \dots, n_{ss}, \\ 0 & \text{otherwise,} \end{cases}$$

and this depends on the concordance parameter r_s through $\rho_s = r_s / (1 - r_s)$. Then the row vectors \mathbf{q}_s^* of matrix \mathbf{Q}^* are a posteriori independently distributed as

$$\mathbf{q}_s^* | \mathbf{X}, r_s, U_s, \dots \stackrel{indep}{\sim} \mathcal{D}_2 \left(\mathbf{n}_s + \frac{\alpha}{2}\mathbf{1} - U_s\mathbf{1}_s \right), \quad \text{where} \\ U_s \stackrel{indep}{\sim} l_s(\cdot), \quad s = 0, 1. \quad (15)$$

Refer to the Appendix for the derivation.

4. Simulation studies

4.1. Cluster-related inferences

As discussed in Section 2.3, the PDP allocations can be interpreted as clusters with unique characteristics. We investigate BaCon’s accuracy as a clustering procedure using simulated covariates for which the true clustering pattern is known. In general, when allocating p objects to an unknown number of clusters using mixture models, the non-identifiability and redundancy of the inferred clusters have been extensively studied (e.g., see Frühwirth-Schnatter, 2006). Some partial solutions are available within the Bayesian paradigm. For example, instead of assuming exchangeable component parameters for finite mixture models, Petralia et al. (2012) invent a repulsive process that leads to a smaller number of better separated and more interpretable clusters. Rousseau and Mengersen (2011) show that in over-fitted finite mixture models, asymptotic emptying of the redundant components is achieved by a carefully chosen prior.

In brain connectome applications, the aforementioned asymptotic results assume that the number of rows of covariate matrix \mathbf{X} remains fixed as the number of columns tends to ∞ . These results do not guarantee that the BaCon model correctly detects even the *number* of covariate clusters. Nevertheless, the following simulation studies suggest a much stronger result: covariates that (do not) cluster under the true process also tend (not) to cluster a posteriori. The key intuition is that if n also grows with p , two covariate column vectors that actually belong to different clusters are eventually separated enough for the BaCon method to allocate them to different clusters. Similarly, the allocations of covariates belonging to the same cluster are correctly called when n and p are both large. This remarkable phenomenon has been documented in other high dimensional settings; Guha and Baladandayuthapani (2016) offer a formal explanation for continuous covariates such as gene expression datasets in cancer research.

4.1.1. Data generated from the BaCon model

Binary covariates for $n = 100$ individuals and $p = 250$ covariates were generated from the proposed model, and the inferred clusters were compared with the truth. The true parameters of the generating model were chosen to approximately match the estimates for the MRN-111 dataset. For each of 25 synthetic datasets, with the true concordance parameters in relation (5), determining cluster separation, taking the values $r_0^{(0)} = r_1^{(0)} \in \{0.875, 0.925, 0.975\}$, the binary covariate matrix \mathbf{X} was generated as follows.:

- (a) **True allocation variables:** We generated partitions $c_1^{(0)}, \dots, c_p^{(0)}$ induced by a PDP with discount parameter $d^{(0)} = 0.4$ and mass parameter $\alpha_1 = 20$. The true number of clusters, Q_0 , was computed for the partition.
- (b) **Latent vector elements:** For $i = 1, \dots, n$ and $k = 1, \dots, Q_0$, we simulated elements $v_{ik}^{(0)} \stackrel{iid}{\sim} \text{Bernoulli}(p^{(0)})$ with $p^{(0)} = 5/7$.
- (c) **Contamination probability matrix:** As indicated in expression (5), for $s = 0, 1$, we generated bivariate vector $\mathbf{q}_s^{*(0)} \stackrel{iid}{\sim} \mathcal{D}_2(1, 1)$. We computed the s th row vector of matrix $\mathbf{Q}^{(0)}$ as $\mathbf{q}_s^{(0)} = (q_{s0}^{(0)}, q_{s1}^{(0)}) = r_s^{(0)} \mathbf{1}_s + (1 - r_s^{(0)}) \mathbf{q}_s^{*(0)}$.
- (d) **Binary covariates:** For individual $i = 1, \dots, n$ and covariate $j = 1, \dots, p$, let the true latent vector element be denoted by g_{ij} . That is, $g_{ij} = v_{ik}^{(0)}$ where $k = c_j^{(0)}$. Each covariate was independently generated as $x_{ij} \sim \text{Bernoulli}(q_{g_{ij}1}^{(0)})$.

There were no responses in this study. Each artificial dataset was analyzed using the BaCon methodology assuming all parameters to be unknown. The accuracy of the inferred covariate-cluster allocation was evaluated by the *proportion of correctly clustered covariate pairs*,

$$\tau = \frac{1}{\binom{p}{2}} \sum_{j_1 \neq j_2 \in \{1, \dots, p\}} \mathcal{I} \left(\mathcal{I}(c_{j_1} = c_{j_2}) = \mathcal{I}(c_{j_1}^{(0)} = c_{j_2}^{(0)}) \right).$$

This measure was estimated as an MCMC empirical average, $\hat{\tau}$, with a high value indicative of high clustering accuracy.

The second column of Table 1 displays the percentage $\hat{\tau}$ for BaCon averaged over the 25 independent replications as cluster separation changes. The posterior inferences

were found to be robust to the contamination levels, i.e., concordance parameter. On average, less than 34.2 pairs were incorrectly clustered out of the $\binom{250}{2} = 31,125$ different covariate pairs, and so $\hat{\tau}$ was greater than 99.89%. Furthermore, in every dataset, \hat{q} , the estimated number of clusters of the least-squares allocation was exactly equal to Q_0 , the true number of PDP clusters.

As a straightforward competitor to the BaCon technique, we applied the k-means algorithm to group the p columns of matrix \mathbf{X} into the true number, Q_0 , of PDP clusters. The percentage of correct allocations, averaged over the 25 independent replications, are displayed in Column 3 of Table 1. Although setting the number of k-means clusters equal to Q_0 gives the k-means algorithm an unrealistic advantage, BaCon significantly outperformed it with respect to clustering accuracy.

We assessed BaCon’s ability to discriminate between PDPs and Dirichlet processes using the log-Bayes factor, $\log(P[d > 0|\mathbf{X}]/P[d = 0|\mathbf{X}])$. With set Θ^* representing all model parameters except d , we obtain by Jensen’s inequality that the log-Bayes factor in favor of PDP models exceeds $E\left(\log\left(\frac{P[d>0|\mathbf{X},\Theta^*]}{p[d=0|\mathbf{X},\Theta^*]}\right) \mid \mathbf{X}\right)$. Unlike the log-Bayes factor, this quantity can be easily estimated using only the post-burn-in MCMC sample. Furthermore, it provides a lower bound for the log-Bayes factor itself, rather than a lower bound for the marginal log-likelihoods from which the log-Bayes factor is derived. The second column of Table 2 displays averages and standard deviations of the log-Bayes factor’s lower bound for the 25 datasets. These numbers correspond to Bayes factors in favor of PDP models significantly exceeding e^{45} , and are extreme evidence in favor of PDP allocations, i.e., the truth.

Reliable posterior inferences were also achieved for the PDP discount parameter, $d \in [0, 1)$. Column 3 of Table 2 displays the 95% posterior credible intervals for d . The posterior inferences are much more precise than the prior, with each CI containing the true value of $d_0 = 0.4$. No posterior mass is assigned to Dirichlet process models in spite of the prior probability, $\Pr(d = 0) = 0.5$.

Asymptotic convergence We compared the estimated and true values of various features of the BaCon model as the number of individuals n and covariates p increased.

Table 1: When the data were generated from the BaCon model, the proportion of correctly clustered covariate pairs for different values of the true concordance parameter for the two competing methods. The standard errors are shown in parentheses.

Concordance parameter	Percent $\hat{\tau}$	
	BaCon	K-Means
0.875	99.890 (0.011)	98.850 (0.165)
0.925	99.896 (0.008)	98.973 (0.119)
0.975	99.891 (0.010)	99.302 (0.116)

Table 2: When the data were generated from the BaCon model, column 2 presents the average lower bound of the log-Bayes factor of PDP models, relative to Dirichlet process models, for different values of the true concordance parameter. Standard deviations for the 25 independent replications are shown in parentheses. Column 3 displays 95 % posterior credible intervals for the PDP discount parameter d .

Concordance parameter	Lower bound of log-BF	95% C.I. for d
0.875	73.232 (13.819)	(0.331, 0.527)
0.925	73.327 (13.250)	(0.332, 0.536)
0.975	80.100 (17.598)	(0.349, 0.541)

Specifically, we implemented the generation and inference strategy described above for the increasing (n, p) tuples, $(20, 50)$, $(50, 125)$, $(70, 175)$, and $(100, 250)$. The results are summarized in Figure 4 for the true concordance parameters $r_0^{(0)} = r_1^{(0)} = 0.925$. The other concordance parameter values exhibited similar trends.

In the left panel of Figure 4, the boxplots display the estimated percentages of correctly clustered covariate pairs, $100\hat{\tau}$, for the 25 simulated datasets. We find that the accuracy of the inferred covariate-cluster allocations increases with data dimension. The right panel of Figure 4 demonstrates the methodology’s success in discriminating between PDPs and Dirichlet processes; the log-Bayes factor lower bounds increasingly favor the true PDP model.

4.1.2. Data generated by a different mechanism

We evaluated inference accuracy under model misspecification. Twenty five datasets were generated using a different process than BaCon. Then, each dataset was analyzed using the BaCon methodology and the inferred clusters were compared with the true

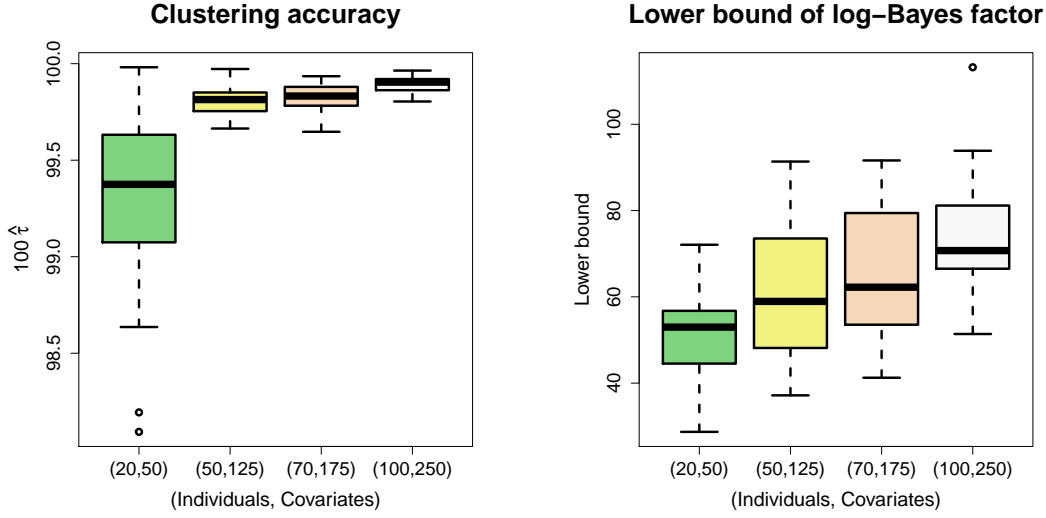


Fig. 4. Posterior inferences for artificial datasets of increasing dimension corresponding to true concordance parameters $r_0^{(0)} = r_1^{(0)} = 0.925$. See the discussion in Section 4.1.

clusters. Specifically, for a true correlation $\varphi^{(0)} \in \{0.90, 0.95, 0.99\}$ determining within-cluster tightness, the binary values of $n = 100$ individuals and $p = 250$ covariates were generated as follows:

- (a) **True number of clusters:** Integer Q_0 was generated from a Poisson distribution with mean $p/8$ and restricted to integers less than $\lfloor p/4 \rfloor$.
- (b) **True allocation variables:** From among the distinct partitions of p objects consisting of exactly Q_0 sets, a partition was uniformly and randomly generated using the R package, `rpartitions`. Allocation variables $c_1^{(0)}, \dots, c_p^{(0)}$ compatible with this partition were randomly generated.
- (c) **Multivariate normal vectors:** Given the cluster allocation variables, for individuals $i = 1, \dots, n$, we independently generated row vectors $\mathbf{z}_i^{(0)}$ of length p from a multivariate normal distribution with mean zero and $p \times p$ variance matrix $\mathbf{\Lambda} = ((\Lambda_{j_1 j_2}))$, where element

$$\Lambda_{j_1 j_2} = \varphi^{(0)} \mathcal{I}(c_{j_1}^{(0)} = c_{j_2}^{(0)}) + (1 - \varphi^{(0)}) \mathcal{I}(j_1 = j_2). \quad (16)$$

Table 3: When the data were generated using the procedure described in Section 4.1.2, the proportion of correctly clustered covariate pairs for two competing methods and different values of the true correlation parameter $\varphi^{(0)}$ in equation (16). The standard errors are shown in parentheses.

Correlation $\varphi^{(0)}$	Percent $\hat{\tau}$	
	BaCon	K-Means
0.90	98.093 (0.329)	94.425 (0.477)
0.95	98.448 (0.253)	94.702 (0.459)
0.99	97.982 (0.315)	94.802 (0.349)

The construct implies that $\text{Var}(z_{ij}^{(0)}) = 1$, so that $\text{Corr}(z_{ij_1}^{(0)}, z_{ij_2}^{(0)}) = \Lambda_{j_1 j_2}$. In particular, the within-cluster correlations of the $z_{ij}^{(0)}$ are equal to $\varphi^{(0)}$, whereas $z_{ij}^{(0)}$ belonging to different clusters are independent.

- (d) **Binary covariates:** For individual $i = 1, \dots, n$ and $j = 1, \dots, p$, we set the binary covariate $x_{ij} = \mathcal{I}(z_{ij}^{(0)} > 0)$.

Each artificial dataset was analyzed using the BaCon and k-means methodologies. The results were relatively robust to the correlation parameter $\varphi^{(0)}$. Averaging over the 25 independent replications, Table 3 displays the estimated percentage of correctly clustered covariate pairs, $\hat{\tau}$, for different values of correlation parameter. In every dataset, the number of clusters detected by BaCon was exactly equal to the true number of clusters, Q_0 . Despite the considerably different data generation mechanism, we found that BaCon was highly accurate in detecting the underlying cluster structure and significantly outperformed the k-means algorithm.

For the lower bound of the log-Bayes factor, previously introduced in Section 4.1.1, the second column of Table 4 displays averages and standard deviations of the MCMC estimates for the 25 datasets. In every situation, the lower bounds of the Bayes factors are significantly greater than $e^6 = 403.4$, implying that the data overwhelmingly favor PDP allocations over Dirichlet processes. Column 3 of Table 4 displays the 95% posterior credible intervals for the PDP discount parameter, d , revealing that no posterior probability was assigned to Dirichlet process models.

Table 4: When the data were generated using the Section 4.1.2 procedure, column 2 presents the average lower bound of the log-Bayes factor of PDP models, relative to Dirichlet process models, for different values of the true correlation parameter $\varphi^{(0)}$ in equation (16). Standard deviations for the 25 independent replications are shown in parentheses. Column 3 displays 95 % posterior credible intervals for the PDP discount parameter d .

Correlation $\varphi^{(0)}$	Lower bound of log-BF	95% C.I. for d
0.90	18.598 (6.930)	(0.178, 0.403)
0.95	16.081 (4.595)	(0.164, 0.392)
0.99	13.949 (4.714)	(0.149, 0.373)

Computational complexity For data generated using a true correlation of $\varphi^{(0)} = 0.9$, we compared the MCMC computational times as the number of individuals n and covariates p increased. All calculations were performed using the University of Florida HiPerGator2 supercomputer, which has 30,000 cores in Intel E5-2698v3 processors with 4 GB of RAM per core and a total storage of 2 petabytes. For the (n, p) pairs, (20, 50), (30, 75), (40, 100), (50, 125), (60, 150), (70, 175), (80, 200), (90, 225), and (100, 250), Figure 5 plots the average computational time per MCMC iteration versus np , the total number of matrix \mathbf{X} elements. The best-fitting straight line is displayed for comparison. For V brain regions, the plot suggests a computational cost of $O(np)$ or $O(nV^2)$ for the MCMC algorithm of Section 3. True correlations of 0.95 and 0.99 had nearly identical results.

4.2. Prediction accuracy

We assessed the prediction accuracy of our methods using $n = 114$ artificially generated continuous responses. However, unlike the previous simulation studies, we used the actual $p = 1,374$ covariates from the MRN-114 dataset. The following procedure was used to generate and analyze 25 sets of subject-specific responses:

- (a) Randomly select 10 covariates with mutual taxicab distances lying between 0.4 and 0.6. This gives the true predictor set $\mathcal{S} \subset \{1, \dots, p\}$ consisting of $|\mathcal{S}| = 10$ members. Recall that for binary covariates, taxicab distances near 0 and 1 correspond to high

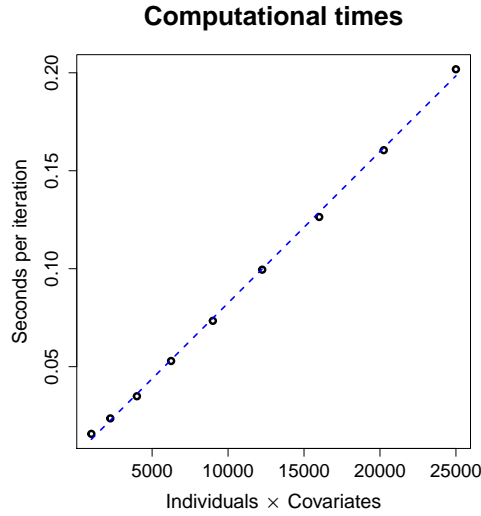


Fig. 5. Computational times for artificial datasets of increasing dimension generated using the process of Section 4.1.2 with true correlation parameter $\varphi^{(0)} = 0.9$. See the discussion in Section 4.1.2.

positive and negative correlations, respectively. Restricting these distances to a neighborhood of 0.5 avoids collinearity in the true predictors, which are unknown at the analysis stage. Nevertheless, there is high collinearity among the $p = 1,374$ *potential* predictors.

(b) For each $\beta^* \in \{0.5, 0.85, 1.2\}$:

For every individual indexed by $i = 1, \dots, n$, generate Gaussian responses y_i with mean $\beta^*/2 + \beta^* \sum_{j \in \mathcal{S}} x_{ij}$ and standard deviation $\sigma_0 = 0.5$. The signal-to-noise ratio in the data increases as β^* increases, with higher values of β^* corresponding to higher associations between the response and true predictors.

(c) Randomly assign 91 individuals (roughly 80%) to the training set and the remaining individuals to the test set.

(d) Apply the BaCon procedure for Gaussian responses to analyze the data. Choose a representative from each cluster as described in option (a) of Section 2.2. Make posterior inferences using the training data and predict the responses for the test case individuals.

Table 5: For different β^* , a comparison of the true positive rate (TPR) and true negative rate (TNR) of the BaCon and K-Means methods.

Coefficient β^*	TPR		TNR	
	BaCon	K-Means	BaCon	K-Means
0.50	54.970 (3.553)	5.600 (1.536)	97.268 (0.279)	93.006 (0.218)
0.85	88.536 (3.195)	7.600 (1.759)	99.189 (0.263)	93.473 (0.199)
1.20	94.208 (1.276)	8.000 (1.732)	99.657 (0.132)	93.210 (0.262)

We fitted the same simulated datasets using the techniques, Lasso (Tibshirani, 1997), L_2 -boosting (Hothorn and Buhlmann, 2006), elastic net (Zou and Trevor, 2005), and random forests (Breiman, 2001). These machine learning techniques are extensively used for binary predictor selection of continuous responses and have been implemented in the R packages glmnet, mboost, and randomForest. We used the default recommended settings for the tuning parameters of these R packages. In choosing these methods, we focused on techniques capable of delivering sparse, interpretable models and quantifying the effects of important brain region pairs.

Because the artificial responses are continuous, the prediction errors of the competing methods were compared using their percentage MSE reduction relative to the null model in the $n^* = 13$ test case individuals. For a given dataset and method, the percentage MSE reduction is equal to $1 - \sum_{i=1}^{n^*} (y_i - \hat{y}_i)^2 / \sum_{i=1}^{n^*} (y_i - \bar{y})^2$, where \hat{y}_i is the method's predicted response for individual i . A large reduction is indicative of a method's high prediction accuracy.

As a straightforward and transparent competitor to the proposed technique, we applied the k-means algorithm to group the p columns of the matrix \mathbf{X} into fewer, say q^* , number of concordant clusters, with q^* chosen to maximize the median percentage MSE reduction over the range $q^* \leq p/4$. Next, for each k-means cluster, we computed the *median potential predictor* as the covariate having the smallest sum of distances to the remaining covariates belonging to the cluster. Finally, from this smaller set of potential predictors, the set of predictors, along with their relationship with the responses, were inferred via L_2 -boosting. We simply refer to this technique as “K-means”.

Table 5 displays the true positive and negative rates for the procedures BaCon and K-Means. For each method, the rates are computed under the notion that we are unable

Table 6: Comparison of the detected model sizes in the simulation study for different β^* .

	$\beta^* = 0.5$	$\beta^* = 0.85$	$\beta^* = 1.2$
BaCon	11.66	10.32	10.23
<i>L</i> ₂ -boosting	36	30	27
Lasso	54	62	71
Elastic net	93	94	95
K-Means	23	24	25

to distinguish between predictors assigned to the same cluster by that method. We find that, for all three levels of the association parameter β^* , the procedure BaCon provides far more accurate inferences than the K-Means procedure.

Figure 6 depicts boxplots of the percentage MSE reductions for the different methods. As expected, the median percentage MSE reductions decrease for most procedures as β^* increases. The only exception is random forests, for which the MSE reductions essentially remain unchanged. The K-means procedure has the highest variability. Irrespective of β^* , the K-means procedure often has high negative percentage MSE reductions, rendering it unusable in practice.

When the true association between the response and true predictors is the weakest (i.e., when $\beta^* = .5$), Lasso performs the best. On the other hand, when the true association is non-negligible, BaCon is the clear winner. Table 6 displays the median number of predictors for each method. Being an MCMC sample average, the estimated model size for BaCon is typically a non-integer. We found that BaCon selects the sparsest models by far, and irrespective of β^* , the detected model size approximately matches the true model size. The other methods detected significantly overfitted models.

In summary, we find that for most reasonable levels of predictor-response association, BaCon strikes the best balance between balances sparsity and prediction. It outperforms competing techniques, with its gains dramatically increasing with the degree of predictor-response association.

5. Data Analysis

Next, we analyzed the motivating MRN-114 connectome dataset. We performed 25 independent replications of the following steps: (i) The data were randomly split in a 4:1

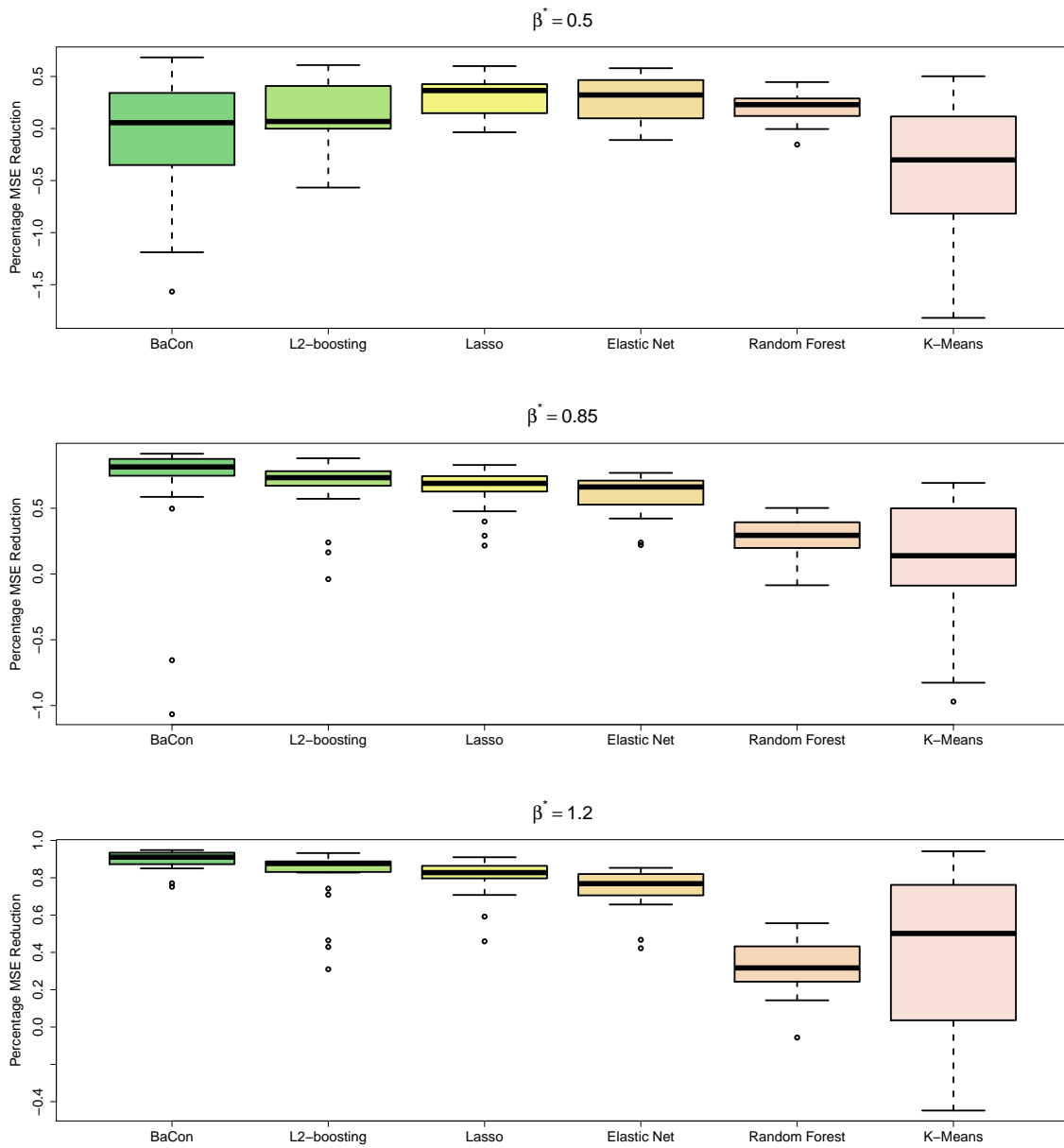


Fig. 6. Side-by-side boxplots comparing the prediction accuracy of the competing techniques in the simulation study of Section 4.2.

ratio into training and test sets. (ii) For the training cases, we analyzed the relationship between the CCI responses and pairwise brain region connectivity as potential predictors using the techniques BaCon, L_2 -boosting, Lasso, elastic net, and random forests. (iii) The five techniques were used to predict the CCI responses of the test cases. For the BaCon procedure, a single covariate representative from each cluster was selected in every MCMC iteration, as described in option (a) of Section 2.2.

Figure 9 displays side-by-side boxplots of the percentage MSE reductions for the different methods. The accuracy and reliability of BaCon are significantly greater than those of Lasso and elastic net. The random forests technique has the highest median accuracy, although it displays fairly high volatility. The results for L_2 -boosting are not shown in the figure because it had a significantly worse performance and a negative median MSE reduction.

The estimated marginal posterior density of the PDP discount parameter d is displayed in Figure 7. The posterior probability of the event $[d = 0]$ is estimated to be exactly zero. This suggests that a non-Dirichlet PDP allocation is strongly supported, as previously suggested by the EDA. As mentioned in Section 3, we computed the *least-squares allocation* for the covariate-to-cluster assignments. The number of clusters in the least-squares allocation was $\hat{q} = 257$. For each least-squares allocation cluster, we computed the taxicab distances between the member covariates and the latent vector. The cluster-specific median distances are plotted in Figure 8. The plots reveal high within-cluster concordance irrespective of cluster size, with the largest clusters having a higher-than-average median taxicab distance. These results demonstrate the effectiveness of BaCon as a model-based clustering procedure.

Table 7 lists seven clusters of pairs of brain regions according to the Desikan atlas that are most predictive of composite creativity index (CCI), for which the cluster-level posterior probabilities of being predictors exceeded 0.8. Although the cluster labels are arbitrary, the clusters appear in decreasing order of posterior probability of being (cluster) predictors, e.g., cluster 1 is the most predictive of CCI. Each cluster consists of one or more brain region pairs, e.g., cluster 1 consists of 5 region pairs, whereas clusters 2 and 3 consist of one pair each. Within each cluster, each brain region pair (i.e.,

Table 7: Top seven clusters of pairs of brain regions that are most predictive of CCI. Each brain region pair in a cluster is listed along with its posterior probability of being a cluster representative. See the text for further discussion.

Cluster	Region 1	Region 2	Probability
1	lh-parsopercularis	lh-entorhinal	0.978
1	lh-parsopercularis	rh-parsorbitalis	0.010
1	lh-parsopercularis	rh-entorhinal	0.006
1	lh-parsopercularis	rh-rostralanteriorcingulate	0.003
1	lh-inferiorparietal	rh-bankssts	0.003
2	lh-parsorbitalis	lh-superiorparietal	1.000
3	lh-caudalmiddlefrontal	lh-lateralorbitofrontal	1.000
4	rh-parsopercularis	rh-temporalpole	0.941
4	rh-parsopercularis	rh-precentral	0.021
4	rh-parsopercularis	rh-supramarginal	0.019
4	rh-parsopercularis	rh-isthmuscingulate	0.019
5	lh-middletemporal	lh-paracentral	1.000
6	lh-rostralmiddlefrontal	lh-MeanThickness	1.000
7	lh-medialorbitofrontal	rh-precuneus	0.764
7	lh-medialorbitofrontal	rh-superiortemporal	0.072
7	lh-superiorfrontal	rh-precuneus	0.038
7	lh-superiorfrontal	rh-caudalmiddlefrontal	0.035
7	lh-medialorbitofrontal	rh-caudalmiddlefrontal	0.033
7	lh-superiorfrontal	rh-cuneus	0.029
7	lh-superiorfrontal	rh-superiortemporal	0.029

covariate) is listed along with its posterior probability of being a cluster representative. For example, the most important brain region pair in cluster 1 is the left hemisphere pair consisting of the regions lh-entorhinal and lh-parsopercularis with a cluster representative posterior probability of 0.978.

These results confirm the findings of Jung et al. (2010, Table 1), who detected regions within the lingual, cuneus, inferior parietal, and cingulate brain regions corresponding to Table 7. Specifically, regions within the so-called “default mode” network are generally associated with creative cognition; particularly, divergent thinking associated with CCI (e.g., medial frontal, precuneus). Our findings are also consistent with the review paper by Jung et al. (2013) that first outlined structural regions comprising the default mode network underlying creative cognition. Finally, a recent meta-analysis (Wu et al., 2015, Tables V and VI) showed both structural and functional correlates of DTT (divergent thinking tasks like CCI) which overlap significantly with our findings.

While the current approach largely supported previous research linking creative cognition to structure and function within the default mode network, other regions were elucidated by this methodology that have not been previously described within structural neuroimaging studies of creative cognition; see Jung et al. (2013) for a review. For example, the preponderance and strength of findings within bilateral inferior frontal lobe, particularly pars opercularis, are relatively novel within the creativity neurosciences. One study of patients suffering from lesions to various brain regions found that lesions to the left inferior frontal gyrus (including pars opercularis and pars triangularis), were found to exhibit high originality scores on divergent thinking tasks (Shamay-Tsoory et al., 2011), suggesting that this hub might be critical to modulation of creative generation. Given that the left inferior gyrus is critical to processing verbal information (Gernsbacher and Kaschak, 2003), this region is also likely to be critical to performance across tasks that are dependent upon verbal output, upon which the vast majority of divergent thinking tasks depend. Support for this notion is found in a study that found regional gray matter volume within the left inferior frontal gyrus (BA 45 - pars opercularis) to be associated with verbal creativity on a divergent thinking task (Zhu et al., 2013).

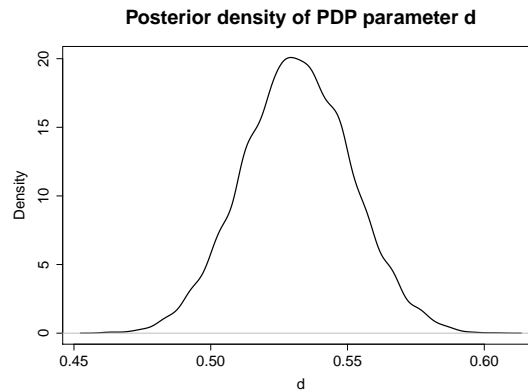


Fig. 7. Posterior summaries for the MRN-114 dataset.

Given that pars opercularis was most often paired with other brain regions in predicting CCI, the BaCon methodology has revealed a central “hub” from which creative cognition (particularly, modulation of originality) might derive. This potential hub has not been previously described in the creativity neuroscience literature, and warrants further research.

6. Conclusions

We focus on the problem of developing accurate predictive models for cognitive traits and neuro-psychiatric disorders using an individual’s brain connection network. We have introduced a class of Bayesian Connectomics (BaCon) models that rely on Poisson-Dirichlet processes to detect a lower-dimensional, bidirectional (covariate, subject) pattern in the adjacency matrix defining brain region connections. This facilitates effective stochastic searches, improved inferences, and test case predictions via spike-and-slab priors for the lower-dimensional cluster predictors. In simulation studies and analyses of the motivating connectome dataset, we find that BaCon performs reliably and accurately compared to established statistical and machine learning procedures. The substantially higher accuracy of BaCon more than compensates for possibly higher clock-times relative to some competitors. The data analysis confirms findings in the literature that have detected associations between creative cognition and the lingual, cuneus, inferior parietal,

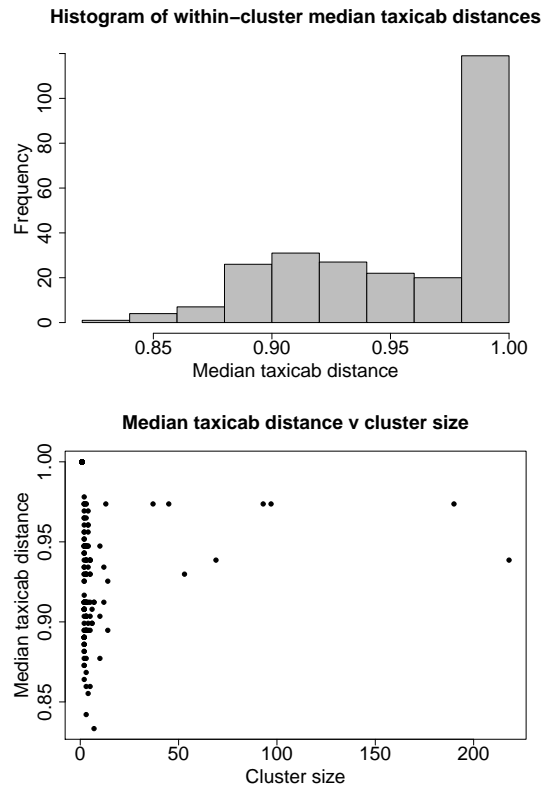


Fig. 8. For the MRN-114 dataset, median taxicab for the $\hat{q} = 257$ PDP clusters of the least-squares allocation.

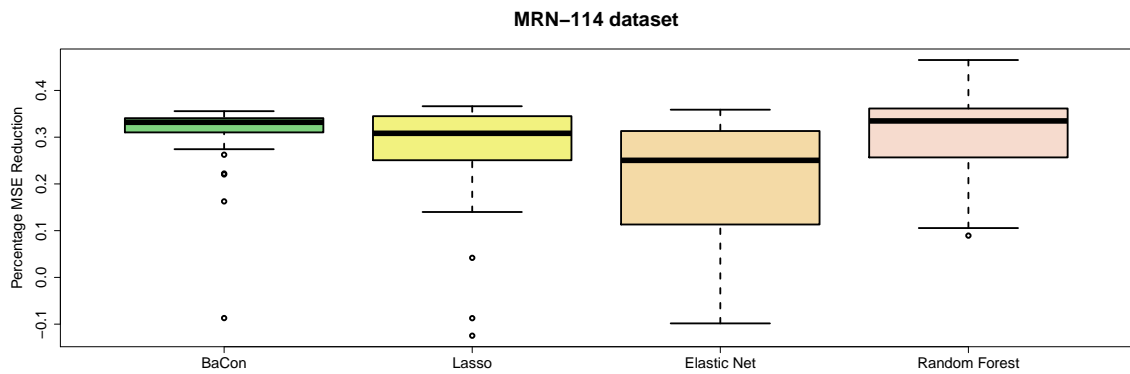


Fig. 9. Side-by-side boxplots comparing the prediction accuracies of different techniques.

and cingulate brain regions. Additionally, the BaCon methodology detects a previously unknown focal point from which modulation of originality, and creative cognition in general, might possibly emanate.

The BaCon methodology in its current form assumes no missing connectivity information. This is, in general, a reasonable assumption given current connectome reconstruction algorithms. A bigger problem than missing data is measurement errors and outlying connectomes due to head movement, problems we will address in future research. Due to the intensive MCMC computations, we have performed the clustering and variable selection parts of BaCon in separate stages, with the second stage relying on the least-squares estimate of the clustering pattern obtained from the first stage. However, the inference procedure is potentially scalable and can be implemented on massively parallel devices such as graphical processing units (GPUs) using fast MCMC algorithms. This would facilitate fully Bayesian posterior inferences via scalable, single-stage implementations of BaCon. In the near future, user-friendly code will be made available on a GitHub repository and through the OpenConnectome project.

Acknowledgments

This work was partially supported by the National Science Foundation under Award DMS-1854003 to SG, and by grant R01MH118927 of the National Institute of Mental Health and grant R01ES027498 of the National Institutes of Environmental Health Sciences, both part of the United States National Institutes of Health, to DD.

Appendix: Derivation of the Gibbs sampler for matrix Q

Updating concordance parameter vector \mathbf{r} . From equation (4), we find that the conditional likelihood function of matrix Q is

$$\begin{aligned} [\mathbf{X} \mid \mathbf{Q}^*, \mathbf{r}, \dots] &= \prod_{i=1}^n \prod_{j=1}^p q_{v_{ic_j}, x_{ij}} = \prod_{s=0,1} \prod_{t=0,1} q_{st}^{n_{st}} \\ &= \prod_{s=0,1} \left\{ (1-r_s)^{n_{s,1-s}} \cdot (q_{s,1-s}^*)^{n_{s,1-s}} \right\} \times \prod_{s=0,1} (r_s + (1-r_s)q_{ss}^*)^{n_{ss}} \end{aligned} \quad (17)$$

Applying the binomial theorem, we obtain

$$\begin{aligned} (r_s + (1-r_s)q_{ss}^*)^{n_{ss}} &= \sum_{v_s=0}^{n_{ss}} \binom{n_{ss}}{v_s} r_s^{v_s} (1-r_s)^{n_{ss}-v_s} (q_{ss}^*)^{n_{ss}-v_s} \\ &= (1-r_s)^{n_{ss}} \sum_{v_s=0}^{n_{ss}} \binom{n_{ss}}{v_s} \rho_s^{v_s} (q_{ss}^*)^{n_{ss}-v_s} \quad \text{where } \rho_s = \frac{r_s}{1-r_s}. \end{aligned}$$

Substituting into equation (17) above gives

$$[\mathbf{X} \mid \mathbf{Q}^*, \mathbf{r}, \dots] = \prod_{s=0,1} \left\{ (1-r_s)^{N_s} \sum_{v_s=0}^{n_{ss}} \binom{n_{ss}}{v_s} \rho_s^{v_s} (q_{ss}^*)^{n_{ss}-v_s} (q_{s,1-s}^*)^{n_{s,1-s}} \right\}. \quad (18)$$

Now the prior for \mathbf{Q}^* in expression (5) is

$$[\mathbf{Q}^*] = \prod_{s=0,1} \frac{1}{B(\frac{\alpha}{2}\mathbf{1})} \prod_{t=0,1} (q_{st}^*)^{\frac{\alpha}{2}-1} \quad (19)$$

Multiplying equations (18) and (19) and marginalizing over matrix \mathbf{Q}^* , we have

$$[\mathbf{X} \mid \mathbf{r}, \dots] = \prod_{s=0,1} \left\{ \sum_{v_s=0}^{n_{ss}} \binom{n_{ss}}{v_s} r_s^{v_s} (1-r_s)^{N_s-v_s} B(\mathbf{n}_s + \frac{\alpha}{2} \mathbf{1} - v_s \mathbf{1}_s) / B(\frac{\alpha}{2} \mathbf{1}) \right\}. \quad (20)$$

Let $f(\cdot \mid r_*, v_s + r_\alpha, N_s - v_s + r_\beta)$ be the density of the left-truncated beta distribution, $\text{beta}(v_s + r_\alpha, N_s - v_s + r_\beta) \cdot \mathcal{I}(r_*, \infty)$. Multiplying the truncated beta priors for the concordance parameters in specification (5) with likelihood expression (20), and including appropriate normalizing constants, we find that the full conditional of the concordance parameters \mathbf{r} is

$$[\mathbf{r} \mid \mathbf{X}, \dots] = \prod_{s=0,1} \left\{ \sum_{v_s=0}^{n_{ss}} h_s(v_s) \cdot f(r_s \mid r_*, v_s + r_\alpha, N_s - v_s + r_\beta) \right\} \quad (21)$$

for the pmf $h_s(\cdot)$ in definition (12). This is equivalent to full conditional (13).

Updating matrix \mathbf{Q}^ conditional on concordance parameter vector \mathbf{r} .* Assuming vector \mathbf{r} to be known, we multiply equations (18) and (19) and normalize to obtain

$$[\mathbf{Q}^* \mid \mathbf{X}, \mathbf{r}, \dots] = \prod_{s=0,1} \left\{ \sum_{v_s=0}^{n_{ss}} l_s(v_s) \cdot \partial_2(\mathbf{q}_s^* \mid \mathbf{n}_s + \frac{\alpha}{2} \mathbf{1} - v_s \mathbf{1}_s) \right\} \quad (22)$$

for the pmf $l_s(\cdot)$ of definition (14), with $\partial_2(\cdot \mid \mathbf{a})$ denoting the density of the Dirichlet distribution, $\mathcal{D}_2(\mathbf{a})$. This is equivalent to full conditional (15).

References

- Albert, J. H. and Chib, S. (1993), “Bayesian Analysis of Binary and Polychotomous Response Data,” *Journal of the American Statistical Association*, 88, 669–679.
- Arden, R., Chavez, R. S., Grazioplene, R., and Jung, R. E. (2010), “Neuroimaging creativity: A psychometric view,” *Behavioural Brain Research*, 214, 143 – 156.
- Barry, D. and Hartigan, J. A. (1993), “A Bayesian analysis for change point problems,” *Journal of the American Statistical Association*, 88, 309–319.
- Benjamini, Y. and Hochberg, Y. (1995), “Controlling the False Discovery Rate: A Practical and Powerful Approach to Multiple Testing,” *Journal of the Royal Statistical Society. Series B (Methodological)*, 57, 289–300.
- Breiman, L. (2001), “Random forests,” *Bayesian Analysis*, 45, 5–32.
- Bressler, S. L. and Menon, V. (2010), “Large-scale brain networks in cognition: emerging methods and principles,” *Trends in Cognitive Sciences*, 14, 277–290.
- Brown, P. J., Vannucci, M., and Fearn, T. (1998), “Multivariate Bayesian variable selection and prediction,” *J. R. Stat. Soc. Series B*, 60, 627–641.
- Bullmore, E. and Sporns, O. (2009), “Complex brain networks: graph theoretical analysis of structural and functional systems,” *Neuroscience*, 10, 186–198.
- Bush, C. A. and MacEachern, S. N. (1996), “A semiparametric Bayesian model for randomised block designs,” *Biometrika*, 83, 275–285.
- Craddock, R. C., Jbabdi, S., Yan, C.-G., Vogelstein, J. T., Castellanos, F. X., Martino, A. D., Kelly, C., Heberlein, K., Colcombe, S., and Milham, M. P. (2013), “Imaging human connectomes at the macroscale,” *Nature Methods*, 10, 524–539.
- Crowley, E. M. (1997), “Product Partition Models for Normal Means,” *Journal of the American Statistical Association*, 92, 192–198.
- Dahl, D. B. (2006), *Model-Based Clustering for Expression Data via a Dirichlet Process Mixture Model*, Cambridge University Press.
- Desikan, R. S., Ségonne, F., Fischl, B., Quinn, B. T., Dickerson, B. C., Blacker, D., Buckner, R. L., Dale, A. M., Maguire, R. P., Hyman, B. T., Albert, M. S., , and Killiany, R. J. (2006), “A Nonparametric Bayesian Technique for High-Dimensional Regression,” *NeuroImage*, 31, 968–980.
- Dunson, D. B. (2009), “Nonparametric Bayes local partition models for random effects,” *Biometrika*, 96, 249–262.
- Dunson, D. B., Herring, A. H., and Engel, S. M. (2008), “Bayesian selection and clustering of polymorphisms in functionally-related genes,” *Journal of the American Statistical Association*, 103, 534–546.
- Dunson, D. B. and Park, J.-H. (2008), “Kernel stick-breaking processes,” *Biometrika*, 95, 307–323.
- Durante, D., Dunson, D. B., et al. (2018), “Bayesian inference and testing of group differences in brain networks,” *Bayesian Analysis*, 13, 29–58.
- Fornito, A., Zalesky, A., and Breakspear, M. (2013), “Graph analysis of the human connectome: Promise, progress, and pitfalls,” *NeuroImage*, 15, 426–444.

- Fraley, C. and Raftery, A. E. (2002), “Model-based clustering, discriminant analysis, and density estimation,” *Journal of the American Statistical Association*, 97, 611–631.
- Freudenberg, J. M., Sivaganesan, S., Wagner, M., and Medvedovic, M. (2010), “A semi-parametric bayesian model for unsupervised differential co-expression analysis,” *BMC Bioinformatics*, 11, 234.
- Frühwirth-Schnatter, S. (2006), *Finite Mixture and Markov Switching Models*, New York: Springer.
- Fuster, J. M. (2000), “The Module: crisis of a paradigm,” *Neuron*, 26, 51–53.
- Genovese, C. R., Lazar, N. A., and Nichols, T. (2002), “Thresholding of Statistical Maps in Functional Neuroimaging Using the False Discovery Rate,” *NeuroImage*, 15, 870–878.
- George, E. and McCulloch, R. (1993), “Variable selection via Gibbs sampling,” *Journal of the American Statistical Association*, 88, 881–889.
- Gernsbacher, M. A. and Kaschak, M. P. (2003), “Neuroimaging studies of language production and comprehension,” *Annual Review of Psychology*, 54, 91–114.
- Gnedin, A. and Pitman, J. (2005), “Regenerative composition structures,” *Annals of Probability*, 33, 445–479.
- Griffin, J. E., Brown, P. J., et al. (2010), “Inference with normal-gamma prior distributions in regression problems,” *Bayesian Analysis*, 5, 171–188.
- Guha, S. and Baladandayuthapani, V. (2016), “A nonparametric Bayesian technique for high-dimensional regression,” *Electronic Journal of Statistics*, 10, 3374–3424.
- Hanson, T. and Johnson, W. O. (2002), “Modeling regression error with a mixture of Polya trees,” *Journal of the American Statistical Association*, 97.
- Hartigan, J. A. (1990), “Partition Models,” *Communications in Statistics, Part A - Theory and Methods*, 19, 2745–2756.
- Harville, D. A. (1977), “Maximum Likelihood Approaches to Variance Component Estimation and to Related Problems,” *Journal of the American Statistical Association*, 72, 320–340.
- Hothorn, T. and Buhlmann, P. (2006), “Model-Based Boosting in High Dimensions,” *Bioinformatics*, 22, 2828–2829.
- Ishwaran, H. and James, L. F. (2003), “Generalized weighted Chinese restaurant processes for species sampling mixture models,” *Statist. Sinica*, 13, 1211–1235.
- Jiang, D., Tang, C., and Zhang, A. (2004), “Clustering Analysis for Gene Expression Data: A Survey,” *IEEE Transactions on Knowledge and Data Engineering*, 16, 1370–1386.
- Jung, R., Mead, B., Carrasco, J., and Flores, R. (2013), “The structure of creative cognition in the human brain,” *Frontiers in Human Neuroscience*, 7, 330.
- Jung, R. E., Segall, J. M., Bockholt, H. J., Flores, R. A., Smith, S. M., Chavez, R. S., and Haier, R. J. (2010), “Neuroanatomy of creativity,” *Human Brain Mapping*, 31, 398–409.
- Kim, S., Tadesse, M. G., and Vannucci, M. (2006), “Variable selection in clustering via Dirichlet process mixture models,” *Biometrika*, 93, 877–893.
- Kundu, S. and Dunson, D. B. (2014), “Bayes variable selection in semiparametric linear models,” *Journal of the American Statistical Association*, 109, 437–447.

- Kuo, L. and Mallick, B. (1997), “Bayesian semiparametric inference for the accelerated failure time model,” *Canadian J. Stat.*, 25, 457–472.
- Lee, J., Müller, P., and Ji, Y. (2013), “A Nonparametric Bayesian Model for Local Clustering,” Tech. rep., Department of Biostatistics, The University of Texas M. D. Anderson Cancer Center.
- Lijoi, A., Mena, R., and Prünster, I. (2007a), “Bayesian nonparametric estimation of the probability of discovering new species,” *Biometrika*, 94, 769–786.
- (2007b), “Controlling the reinforcement in Bayesian nonparametric mixture models,” *Journal of the Royal Statistical Society: Series B (Statistical Methodology)*, 69, 715–740.
- Lijoi, A. and Prünster, I. (2010), *Models beyond the Dirichlet process*, Cambridge Series in Statistical and Probabilistic Mathematics, pp. 80–136.
- Liu, M., Zhang, Z., and Dunson, D. B. (2019), “Auto-encoding graph-valued data with applications to brain connectomes,” *arXiv preprint arXiv:1911.02728*.
- MacLehose, R. F. and Dunson, D. B. (2010), “Bayesian semiparametric multiple shrinkage,” *Biometrics*, 66, 455–462.
- Medvedovic, M., Yeung, K. Y., and Bumgarner, R. E. (2004), “Bayesian mixture model based clustering of replicated microarray data,” *Bioinformatics*, 20, 1222–1232.
- Müller, P. and Mitra, R. (2013), “Bayesian nonparametric inference—why and how,” *Bayesian analysis (Online)*, 8.
- O’Hara, R. B. and Sillanpää, M. J. (2009), “A review of Bayesian variable selection methods: what, how and which,” *Bayesian Analysis*, 4, 85–117.
- Park, T. and Casella, G. (2008), “The Bayesian Lasso,” *Journal of the American Statistical Association*, 103, 681–686.
- Perman, M., Pitman, J., and Yor, M. (1992), “Size-biased sampling of Poisson point processes and excursions,” *Probab. Theory Related Fields*, 92, 21–39.
- Petralia, F., Rao, V., and Dunson, D. B. (2012), “Repulsive Mixtures,” *ArXiv e-prints*.
- Pitman, J. (1995), “Exchangeable and partially exchangeable random partitions,” *Probab. Theory Related Fields*, 102, 145–158.
- Pitman, J. and Yor, M. (1997), “The two-parameter Poisson-Dirichlet distribution derived from a stable subordinator,” *Ann. Probab.*, 25, 855–900.
- Quintana, F. A. (2006), “A predictive view of Bayesian clustering,” *Journal of Statistical Planning and Inference*, 136, 2407–2429.
- Quintana, F. A. and Iglesias, P. L. (2003), “Bayesian clustering and product partition models,” *J. R. Statist. Soc. B*, 65, 557–574.
- Roncal, W. G., Koterba, Z. H., Mhembere, D., Kleissas, D. M., Vogelstein, J. T., Burns, R., Bowles, A. R., Donavos, D. K., Ryman, S., Jung, R. E., Wu, L and, C. V., and Vogelstein, R. J. (2013), “MIGRAINE: MRI Graph Reliability Analysis and Inference for Connectomics,” *IEEE Global Conference on Signal and Information Processing*.
- Rousseau, J. and Mengersen, K. (2011), “Asymptotic behaviour of the posterior distribution in overfitted mixture models,” *Journal of the Royal Statistical Society: Series B*, 73, 689–710.

- Rubinov, M. and Sporns, O. (2010), “Complex network measures of brain connectivity: Uses and interpretations,” *NeuroImage*, 52, 1059–1069.
- Shamay-Tsoory, S. G., Adler, N., Aharon-Peretz, J., Perry, D., and Mayseless, N. (2011), “The origins of originality: the neural bases of creative thinking and originality,” *Neuropsychologia*, 29, 178–185.
- Stam, C. J. (2014), “Modern network science of neurological disorders,” *Nature Reviews Neuroscience*, 15, 683–695.
- Stirling, J. and Elliott, R. (2008), *Introducing Neuropsychology*, Routledge.
- Tibshirani, R. (1997), “The lasso method for variable selection in the Cox model,” *Stat. Med.*, 16, 385–395.
- Wang, J., He, L., Zheng, H., and Lu, Z.-L. (2014), “Optimizing the Magnetization- Prepared Rapid Gradient-Echo (MP-RAGE) Sequence,” *PLoS ONE*, 9, 1–12.
- Weisberg, S. (1985), *Applied Linear Regression*, J. Wiley and Sons, NY.
- Wu, X., Yang, W., Tong, D., Sun, J., Chen, Q., Wei, D., Zhang, Q., Zhang, M., and Qi, J. (2015), “A Meta-Analysis of Neuroimaging Studies on Divergent Thinking Using Activation Likelihood Estimation,” *Human Brain Mapping*, 36, 2703–2718.
- Xu, X., Ghosh, M., et al. (2015), “Bayesian Variable Selection and Estimation for Group Lasso,” *Bayesian Analysis*.
- Yengo, L., Jacques, J., and Biernacki, C. (2014), “Variable clustering in high dimensional linear regression models,” .
- Zalesky, A., Fornito, A., and Bullmore, E. T. (2010), “Network-based statistic: Identifying differences in brain networks,” *NeuroImage*, 53, 1197–1207.
- Zeger, S. L. and Karim, M. R. (1991), “Generalized linear models with random effects: A Gibbs sampling approach,” *Journal of the American Statistical Association*, 86, 79–86.
- Zhu, F., Zhang, Q., and Qiu, J. (2013), “Relating inter-individual differences in verbal creative thinking to cerebral structures: An optimal voxel-based morphometry study,” *PLoS ONE*, 8, e79272.
- Zou, H. and Trevor, T. (2005), “Regularization and Variable Selection via the Elastic Net,” *Journal of the Royal Statistical Society, Series B*, 67, 301–320.